

**Fluoride-Ion Solvation In Non-Aqueous Electrolyte Solutions**  
**Invitation to contribute to a special collection in honour of**  
**Prof. Grubbs' 50 years of career**

Journal:	<i>Materials Chemistry Frontiers</i>
Manuscript ID	QM-RES-08-2019-000512.R1
Article Type:	Research Article
Date Submitted by the Author:	11-Oct-2019
Complete List of Authors:	Davis, Victoria K.; NASA Jet Propulsion Laboratory, Electrochemical Technologies Group Munoz, Stephen; California Institute of Technology Division of Chemistry and Chemical Engineering Kim, Jeongmin; California Institute of Technology Division of Chemistry and Chemical Engineering Bates, Christopher; California Institute of Technology Division of Chemistry and Chemical Engineering Momčilović, Nebojša; California Institute of Technology Division of Chemistry and Chemical Engineering Billings, Keith; NASA Jet Propulsion Laboratory, Electrochemical Technologies Group Miller, Thomas; California Institute of Technology Division of Chemistry and Chemical Engineering Grubbs, Robert; California Institute of Technology Division of Chemistry and Chemical Engineering Jones, Simon; NASA Jet Propulsion Laboratory, Electrochemical Technologies Group

# Fluoride-Ion Solvation In Non-Aqueous Electrolyte Solutions

Victoria K. Davis,<sup>a</sup> Stephen Munoz,<sup>b</sup> Jeongmin Kim,<sup>b</sup> Christopher M. Bates,<sup>b†</sup> Nebojša Momčilović,<sup>b</sup> Keith J. Billings,<sup>a</sup> Thomas F. Miller III,<sup>b</sup> Robert H. Grubbs,<sup>b</sup> Simon C. Jones<sup>a\*</sup>

<sup>a</sup>Electrochemical Technologies Group, Jet Propulsion Laboratory, California Institute of Technology, Pasadena, California 91109, United States.

<sup>b</sup>Division of Chemistry and Chemical Engineering, California Institute of Technology, Pasadena, California 91125, United States.

\*Corresponding author: Email: [scjones@caltech.edu](mailto:scjones@caltech.edu)

†Present address: Departments of Materials, Chemical Engineering, and Chemistry & Biochemistry, University of California, Santa Barbara, Santa Barbara, California 93106, United States.

## Abstract

Understanding the factors that influence ion-solvent properties for the fluoride ion in organic solvents is key to the development of useful liquid electrolytes for fluoride-ion batteries. Using both experimental and computational methods, we examined a range of chemical and electrochemical properties for a set of organic solvents in combination with dry *N,N,N*-trimethylneopentylammonium fluoride ( $\text{Np}_1\text{F}$ ) salt. Results showed that solvent electronic structure strongly influences  $\text{Np}_1\text{F}$  dissolution, and the  $\text{p}K_a$  of solvent protons provides a good guide to potential  $\text{F}^-$  reactivity. We found a number of organic solvents capable of dissolving  $\text{Np}_1\text{F}$  while providing chemically-stable  $\text{F}^-$  in solution and characterized three of them in detail: propionitrile (PN), 2,6-difluoropyridine (DFP), and bis(2,2,2-trifluoroethyl) ether (BTFE). Arrhenius analysis for  $\text{Np}_1\text{F}/\text{PN}$ ,  $\text{Np}_1\text{F}/\text{DFP}$ , and  $\text{Np}_1\text{F}/\text{BTFE}$  electrolytes suggests that DFP facilitates the highest  $\text{F}^-$  ion mobility of the three neat solvents. Electrolyte mixtures of BTFE and amide co-solvents exhibit higher ionic conductivity than the neat solvents. This improved ionic conductivity is attributed to the ability of BTFE:co-solvent mixtures to partition between  $\text{Np}_1^+$  and  $\text{F}^-$  ion-aggregates, promoting better ion dissociation.

## Introduction

Fluoride-ion batteries (FIBs) have traditionally been fabricated using solid-state electrolytes.<sup>1</sup> An ideal battery electrolyte must exhibit both fast ion transport (e.g., *via* high concentrations of mobile ions) and robust chemical stability. Solid-state  $\text{F}^-$ -conducting electrolytes can be extremely stable, but typically operate at elevated temperatures ( $\geq 150$  °C) due to a high activation barrier for ion movement in the solid lattice; although, we note that a solid-state FIB operating at room temperature (RT) has recently been described.<sup>2,3</sup> In contrast, liquid electrolytes can offer much-higher RT ionic conductivity due to the presence of mobile ions in solution; however the formulation of a liquid electrolyte containing a significant concentration of chemically-stable  $\text{F}^-$  ions has

traditionally been a considerable challenge in a number of fields including chemical synthesis, ion recognition and electrochemistry.<sup>4–10</sup>

We recently reported a non-aqueous liquid FIB electrolyte, where high salt concentration (>2M) was achieved in bis(2,2,2-trifluoroethyl) ether (BTFE) solvent using *N,N,N*-trimethylneopentylammonium fluoride ( $\text{Np}_1\text{F}$ ) and *N,N,N*-dimethyldineopentylammonium fluoride ( $\text{Np}_2\text{F}$ ) salts.<sup>11</sup> Herein, we probe ion–solvent and ion–ion interactions in a range of different dry organic solvents using  $\text{Np}_1\text{F}$  with the aim of identifying common solvent properties that stabilize  $\text{F}^-$  in solution while also facilitating rapid ion transport and high ionic conductivity. Determining the key factors that dictate  $\text{F}^-$ -ion solvation will help further the understanding of this new class of liquid electrolytes and point towards improved formulations.

## Experimental

### Solvent Screening

Studies were carried out inside an Ar-filled glovebox ( $\text{H}_2\text{O} \leq 10$  ppm). Solvents were purchased from commercial sources and dried over 4 Å molecular sieves, monitored by Karl Fischer titration. Solvent purity was confirmed via  $^1\text{H}$  and/or  $^{19}\text{F}$  NMR spectroscopy prior to experiments. Solvent screening was carried out by dissolving dry  $\text{Np}_1\text{F}$  in the solvent until the solution appeared to be saturated. Masses of oven-dried scintillation vials, solvent, and  $\text{Np}_1\text{F}$  were recorded using an analytical balance inside the glovebox, enabling approximate saturation concentrations (M) of  $\text{Np}_1\text{F}$  in the solvent to be determined.

### Nuclear Magnetic Resonance (NMR) Spectroscopy

NMR spectra were obtained using either a Mercury Plus 300, Varian 400, or Inova 500 spectrometer. Chemical shifts for protons ( $^1\text{H}$ ) are reported in parts per million downfield from tetramethylsilane and are referenced to residual protium in the NMR solvent,  $\text{CD}_3\text{CN}$  ( $\delta = 1.96$  ppm). Chemical shifts for fluorine ( $^{19}\text{F}$ ) are reported in parts per million and are referenced to deuterated bifluoride signal,  $\text{DF}_2^-$  ( $\Phi = -147.0$  ppm).

### Computational Methods

Molecular geometries were optimized at the B3LYP-D3/def2-TZVP level of theory using the ORCA software package<sup>12</sup> and additional quantum chemistry calculations were performed using both ORCA and the *entos* software package.<sup>13</sup> All-atom simulations were performed using the LAMMPS software package. Detailed methods for partial charges,  $\text{p}K_a$  values, free energy of solvation, mixed-solvent MD simulations, and diffusion constants are described in the ESI.

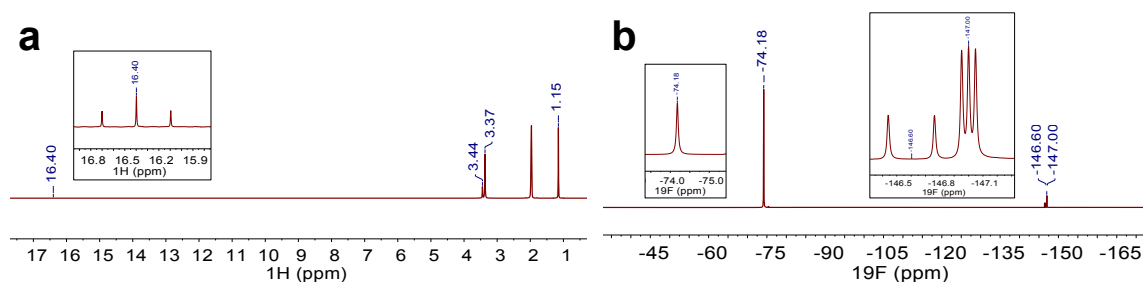
### Ionic Conductivity

Ionic conductivities were investigated by AC impedance spectroscopy using a VersaSTAT potentiostat. Measurements were acquired between 100 mHz and 1 MHz using an air-free glass conductivity cell with a Teflon ring sealing the solution between two parallel Pt electrodes (1 cm separation). The cell constant was determined before each experiment by measuring the conductivity of an aqueous potassium chloride (0.1 M) solution. Thermal control was provided by a Tenney TUJR chamber, with the sample allowed to reach thermal equilibrium before measurement (as determined by no observed change in the impedance spectrum over time).

## Results & discussion

### Solubility and Chemical Stability

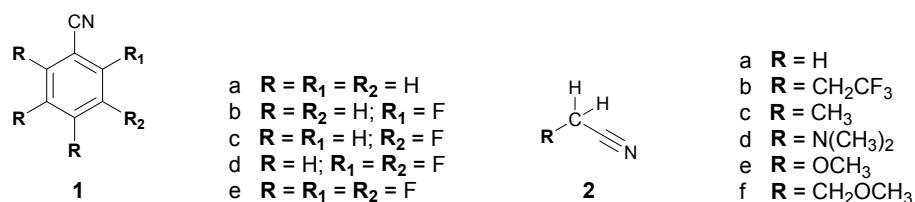
Acetonitrile is typically an excellent choice for an organic electrolyte solvent due to its high salt solubility, good dielectric permittivity and low viscosity.<sup>14</sup> Indeed, a high solubility (2.18 M) of  $\text{Np}_1\text{F}$  can be achieved in acetonitrile.<sup>11</sup> However, due to its strong basicity, fluoride ( $\text{F}^-$ ) reacts with the weakly-acidic protons of acetonitrile to form bifluoride,  $\text{HF}_2^-$ .<sup>15</sup>  $^1\text{H}$  and  $^{19}\text{F}$  NMR in  $d_6$ -acetonitrile of the  $\text{Np}_1\text{F}/\text{CH}_3\text{CN}$  solution shows the characteristic peaks for both  $\text{HF}_2^-$  and deuterated bifluoride,  $\text{DF}_2^-$  (Fig. 1); here,  $\text{F}^-$  has reacted with both  $\text{CH}_3\text{CN}$  and  $\text{CD}_3\text{CN}$  (NMR solvent).



**Figure 1.** (a)  $^1\text{H}$  NMR and (b)  $^{19}\text{F}$  NMR spectra of  $\text{Np}_1\text{F}$  (2.18 M) in  $\text{CH}_3\text{CN}$  using  $\text{CD}_3\text{CN}$  NMR solvent.

In our screening studies, we considered the appearance of  $\text{HF}_2^-$  (1:2:1 triplet,  $\delta \sim 16.3$  ppm in  $^1\text{H}$  NMR; 1:1 doublet,  $\Phi \sim -146.6$  ppm,  $^1J_{\text{HF}} = 121$  Hz in  $^{19}\text{F}$  NMR) as a marker indicating reaction of  $\text{F}^-$  with the solvent of interest. As we used  $\text{CD}_3\text{CN}$  as the NMR solvent, we expected to see the  $\text{DF}_2^-$  signal in all cases (1:1:1 triplet,  $\Phi \sim -147.0$  ppm,  $^1J_{\text{DF}} = 18$  Hz in  $^{19}\text{F}$  NMR) if significant  $\text{F}^-$  was present in solution. Note that  $\text{HF}_2^-$  and  $\text{DF}_2^-$  do not exchange on the NMR timescale at RT, so the presence of  $\text{DF}_2^-$  was assumed not to interfere with the screening process.<sup>5,15</sup>

We investigated the solubility of  $\text{Np}_1\text{F}$  in a number of aromatic nitriles as, typically, aromatic protons are much less acidic ( $\text{p}K_{\text{a}} = 43 - 45$ ) than those of acetonitrile ( $\text{p}K_{\text{a}} = 31.3$ ), so such materials might be expected to show greater stability.<sup>16</sup> Table 1 shows the solubility of  $\text{Np}_1\text{F}$  in benzonitrile (BN) and benzonitrile-derivatives.

**Table 1. Effect of aromatic (1) or aliphatic (2) nitrile solvent structure on  $\text{Np}_1\text{F}$  solubility and  $\text{F}^-$  reactivity**

Entry	Solvent	Solubility <sup>a</sup> (M)	Ratio <sup>b</sup> $\text{F}^- : \text{HF}_2^-$	Calculated $\text{pK}_a$
1a	BN	0.00	N/A	44
1b	2-FBN	0.12	1 : 0.00	39
1c	3-FBN	0.19	1 : 0.00	37
1d	2,3-FBN	0.40	— <sup>c</sup>	40
1e	$\text{F}_5\text{BN}$	0.00	N/A	N/A
2a	AN	2.18	1 : 0.58	31
2b	TFBN	0.10	1 : 0.58	27
2c	PN	0.07	1 : 0.00	33
2d	DMAAN	0.14	— <sup>c</sup>	35
2e	MeOAN	0.80	1 : 0.01	32
2f	MeOPN	0.78	1 : 0.16	29

<sup>a</sup>Solubility reported as moles of  $\text{Np}_1\text{F}$  per liter solvent. <sup>b</sup>Determined from integrated areas of  $^{19}\text{F}$  NMR peaks. <sup>c</sup>2,3-FBN and DMAAN solvents used were not able to be dried effectively.

$\text{Np}_1\text{F}$  was found to be completely insoluble in both fully-protiated (BN) and fully-fluorinated ( $\text{F}_5\text{BN}$ ) benzonitriles. However, salt dissolution could be achieved in 2-fluorobenzonitrile (2-FBN), 3-fluorobenzonitrile (3-FBN) and 2,3-difluorobenzonitrile (2,3-FBN). These results indicate that *partial* fluorination of the solvent is helpful to solubilize the tetraalkylammonium fluoride salt. Unfortunately, in all of these solvents multiple new  $^{19}\text{F}$  NMR peaks were observed upon  $\text{Np}_1\text{F}$  dissolution, leading to ambiguity in assigning the signal from  $\text{F}^-$  in solution (see Fig. S1 for an example spectrum), and limiting any conclusions that could be made regarding long-term chemical stability.

We then evaluated substituted aliphatic nitriles and found that, in contrast to the aromatic nitriles, the  $\text{F}^-$  NMR signal was clean and easily-assigned (see Fig. S2 and Fig. S3 for examples). 4,4,4-trifluorobutyronitrile (TFBN) demonstrated limited solubility, although  $\text{HF}_2^-$  formation was as pronounced as for acetonitrile. In contrast, non-fluorinated propionitrile (PN) dissolved a similar amount of salt with the advantage of excellent chemical stability.<sup>11</sup> We hypothesized this enhanced stability arose from

increasing electron-rich character of the protons  $\alpha$ -to the nitrile group; consistent with this, moving to more polar (*N,N*-dimethylamino)acetonitrile (DMAAN) improved solubility with similar chemical stability observed. Further increasing solvent polarity using methoxyacetonitrile (MeOAN) and 3-methoxypropionitrile (MeOPN) could push salt solubility to greater values at the expense of chemical stability. Indeed,  $^1\text{H}$  NMR analysis of the  $\text{F}^-/\text{MeOPN}$  solution (Fig. 2) offered clear evidence for the presence of  $\text{HF}_2^-$ , acrylonitrile and methanol, indicating that this solvent is unstable to  $\text{F}^-$ -promoted elimination as outlined in Scheme 1.

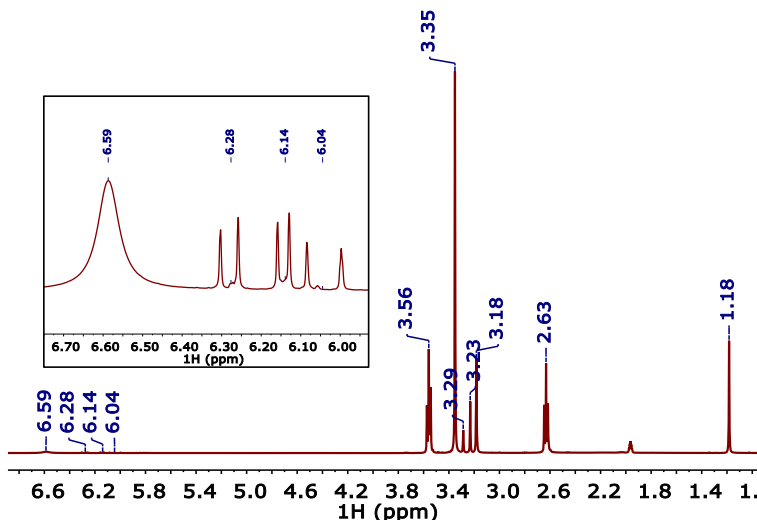
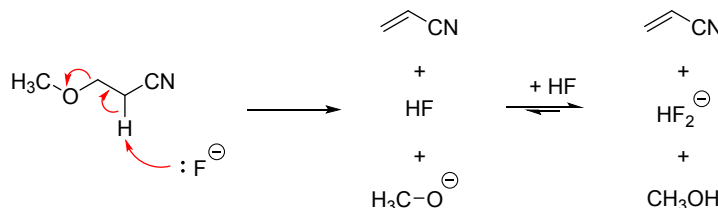


**Figure 2.**  $^1\text{H}$  NMR spectrum of  $\text{Np}_1\text{F}$  (0.78 M) in MeOPN in  $\text{CD}_3\text{CN}$ . New peaks appear at  $\delta$  6.04 (1H, dd), 6.14 (1H, dd), and 6.28 (1H, dd) indicative of acrylonitrile, and at  $\delta$  3.18 (3H, s) and 6.59 (1H, bs) consistent with methanol.



**Scheme 1.** Proposed mechanism for  $\text{F}^-$ -enabled decomposition of 3-methoxypropionitrile.

We calculated  $\text{p}K_a$  values for each nitrile solvent using Density Functional Theory (DFT), and these are reported in Table 1; the value obtained for BN by DFT was consistent with the literature value ( $\text{p}K_a = 45$ ).<sup>16</sup> These calculated  $\text{p}K_a$ s are well-correlated with the observation of  $\text{HF}_2^-$  formation below a certain critical value, and DFT indicated that, for all the aliphatic nitriles considered, the  $\alpha$ -cyano protons are the most likely to be deprotonated by  $\text{F}^-$ . Consistent with this, TFBN, MeOPN, and AN have the most-acidic  $\text{CH}_2$  protons and displayed the greatest extent of  $\text{HF}_2^-$  formation. Hence, we conclude that solvents with  $\text{p}K_a \geq 33$  are not deprotonated by  $\text{F}^-$  ions at room temperature so can be considered chemically-stable in the absence of other decomposition pathways.

As partial solvent fluorination appeared to be a useful strategy for salt dissolution, we also examined a number of commercially-available non-nitrile materials. Table 2 shows solvent screening results with partially fluorinated solvents 2,6-difluoropyridine (2,6-DFP), fluoroethylene carbonate (FEC), 2,2,2-trifluoroacetophenone (TFAP) and phenyltrifluoroacetate (PhTFA), as well as a variety containing the  $\text{O}-\text{CH}_2-\text{CF}_3$  functionality: 2,2,2-trifluoroethyl trifluoroacetate (TFE-TFA), bis(2,2,2-trifluoroethyl)

carbonate (BTFC), bis(2,2,2-trifluoroethyl) ether (BTFE), and tris(2,2,2-trifluoroethyl) phosphite (TTFP).

**Table 2. F<sup>-</sup> stability and <sup>19</sup>F NMR characteristics for Np<sub>1</sub>F in partially-fluorinated organic solvents**

Solvent	Number of O-CH <sub>2</sub> -CF <sub>3</sub> moieties	Solubility (M) <sup>a</sup>	F <sup>-</sup> chemical shift (ppm) <sup>b</sup>	HF <sub>2</sub> <sup>-</sup> chemical shift (ppm) <sup>b</sup>
TFAP	0	0.00	—	—
2,6-DFP	0	0.39	-76.12 (25)	—
PhTFA	0	0.47	N.A. <sup>c</sup>	-147 (bs) <sup>d</sup> [15.88] <sup>e</sup>
FEC	0	0.71	N.A. <sup>c</sup>	-147 (bs) <sup>d</sup> [14.97] <sup>e</sup>
TFE-TFA	1	0.95	N.A. <sup>f</sup>	-146.61
BTFC	2	0.19	N.A. <sup>f</sup>	-146.50
BTFE	2	2.23	-71.94 (25)	—
TTFP	3	1.05	N.A. <sup>f</sup>	—

<sup>a</sup>Solubility reported as moles of Np<sub>1</sub>F per liter solvent. <sup>b</sup>Determined by <sup>19</sup>F NMR normalized to DF<sub>2</sub><sup>-</sup> reference. Peak width at half height (Hz) reported in parenthesis. <sup>c</sup>No F<sup>-</sup> peak detected. <sup>d</sup>Broad singlet observed in the <sup>19</sup>F NMR due to HF<sub>2</sub><sup>-</sup> and DF<sub>2</sub><sup>-</sup> signal overlap. <sup>e</sup><sup>1</sup>H HF<sub>2</sub><sup>-</sup> chemical shift. <sup>f</sup>N.A. = not assigned due to appearance of multiple new peaks in <sup>19</sup>F NMR upon addition of Np<sub>1</sub>F to solvent (see NMR spectra in the ESI).

As Table 2 suggests, increasing numbers of O-CH<sub>2</sub>-CF<sub>3</sub> moieties can aid Np<sub>1</sub>F dissolution, although F<sup>-</sup> reactivity is also high in many cases (PhTFA, FEC, TFE-TFA, BTFC and TTFP). Only 2,6-DFP and BTFE were found to solvate F<sup>-</sup> without reacting, and clearly BTFE appears superior in terms of absolute salt solubility. Table S1 provides a summary of all the solvent screening results described, and representative NMR spectra are shown in Fig. S1 through S8.

To gain greater insight into the structural features helpful for fluoride salt dissolution, we performed a series of computational studies. First, using molecular dynamics (MD), we calculated the free energies of solvation for F<sup>-</sup> and Np<sub>1</sub><sup>+</sup> ions in a selected number of solvents (Table S2) across the spectrum from non-solvating (F<sub>5</sub>BN) through weakly-solvating (PN) to strongly-solvating (2,3-FBN, 2,6-DPF and BTFE). Clearly, the difference between good and poor solvents is evident from the significant gap in the sum of free energies of solvation calculated (Table S2). Indeed, F<sub>5</sub>BN demonstrates a higher free energy of solvation for Np<sub>1</sub><sup>+</sup> than for F<sup>-</sup>, unlike the other species investigated which all show higher F<sup>-</sup> solvation energies (Fig. 3a). 2,3-FBN would appear to be a good solvent from this analysis, although the ambiguous <sup>19</sup>F NMR spectrum observed experimentally renders this result questionable in practice. For 2,6-DFP and PN, the calculated solvation free energies correlate well with their experimental solubility trends (i.e., 2,6-DFP > PN) although the values for BTFE suggest that it might be a worse solvent than the other two (for all three solvents, stable F<sup>-</sup> was clearly observed by <sup>19</sup>F NMR

spectroscopy). However, the MD snapshots and partial charge calculations provide insight into the strong performance of BTFE at finite salt concentrations in the experiments.

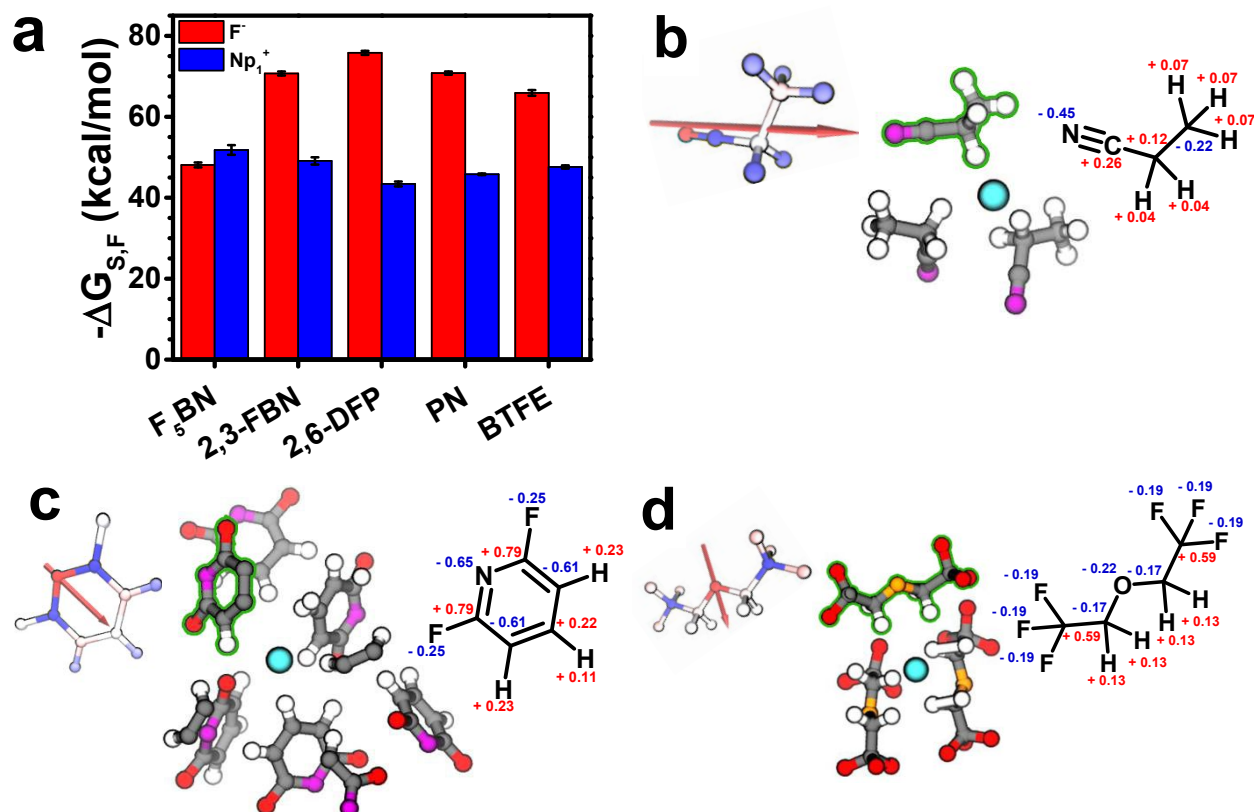


**Figure 3.** Computational simulations for ions in  $F_5BN$ , 2,3-FBN, 2,6-DFP, PN, and BTFE. (a) Comparison of ion solvation free energies. Data are means  $\pm$  standard deviation. Illustration of solvent properties for (b) PN, (c) 2,6-DFP, and (d) BTFE. The middle image represents a simulated solvation shell of solvent molecules surrounding  $F^-$  (cyan sphere). The left image shows the dipole orientation of the solvent molecule outlined in green. Vectors are drawn from negative to positive (not to scale). Dipole magnitudes are  $\mu = 4.1$  D (PN),  $\mu = 3.77$  D (2,6-DFP) and  $\mu = 3.46$  D (BTFE). The right image shows the partial charge distribution of the solvent molecule oriented in the same direction as the solvent molecule outlined in green.

Computationally generated images of ion solvation, solvent dipole moment, and partial charge distribution for PN (Fig. 3b), 2,6-DFP (Fig. 3c), and BTFE (Fig. 3d) from these MD simulations are shown (similar solvation images for 2,3-FBN (Fig. S9a) and  $F_5BN$  (Fig. S9b) can be found in the ESI). For PN, the  $F^-$  solvation environment consists mainly of  $CH_2$ -moieties  $\alpha$ - to the nitrile group, with minor terminal  $CH_3$  participation; the  $Np_1^+$  solvation environment is more complicated, but there is significant participation of the nitrile group. For 2,6-DFP, the protons *para*- and *meta*- to the ring nitrogen have the dominant role in the solvation environment for the  $F^-$  ions; the nitrogen and fluorine atoms dictate solvation of the  $Np_1^+$  ion.

In BTFE,  $F^-$ -solvation is dominated by the  $CH_2^-$  groups which separate the oxygen and  $CF_3$  moieties;<sup>11</sup>  $Np_1^+$  ion solvation sites are characterized mainly by terminal  $CF_3$  groups. However, when the 3D orientation of solvent molecules around  $F^-$  and  $Np_1^+$  ions simultaneously is considered, the greater solvating power of BTFE is suggested. BTFE is much more conformationally flexible than PN or 2,6-DFP, and is not constrained to a single plane in space. This allows for a closer chelating interaction with (and separation between) anions and cations. Similarly, the partial charge distribution of BTFE creates two

oppositely charged polar regions across the molecule. In MD solvation snapshots, we observed the positive pole of BTFE to be oriented toward  $F^-$ , leaving the negative pole available for solvation of  $Np_1^+$ ; BTFE thus promotes dissolution of the  $Np_1F$  salt by inserting itself between ions to create a compact solvation environment. Hence, in general, we conclude that a favorable partial charge distribution (e.g., associated with structural features such as  $-O-CH_2-CF_3$ ) and a high degree of conformational flexibility are beneficial features for a solvent to exhibit high solubility of alkylammonium fluoride salts.

### Ionic Conductivity

Variable temperature ionic conductivity measurements were performed for solutions of  $Np_1F$  in PN, 2,6-DFP and BTFE (Fig. 4).

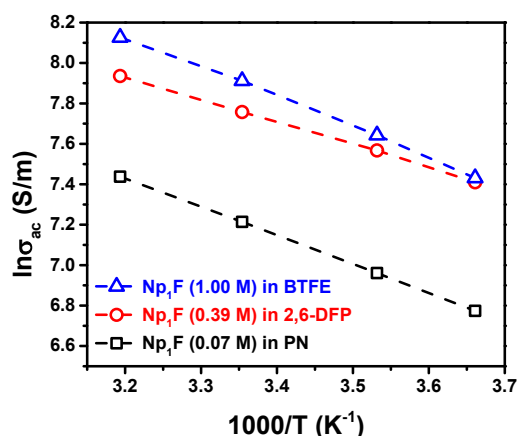


**Figure 4.** Variable temperature ionic conductivity of  $Np_1F$  in PN, 2,6-DFP, and BTFE solvents.

Arrhenius analysis gives activation energies for ionic conductivity in  $Np_1F$  (0.07 M)/PN,  $Np_1F$  (0.39 M)/2,6-DFP, and  $Np_1F$  (1.00 M)/BTFE as 11.8, 9.3, and 12.4 kJ/mol, respectively. 2,6-DFP demonstrated the lowest activation barrier for ionic conductivity, indicating that 2,6-DFP facilitates better  $F^-$  ion mobility in solution. Indeed, we found that addition of 2,6-DFP to  $Np_1$ /BTFE mixtures increased the ionic conductivity of the solution: values for  $Np_1F$  (0.75 M)/BTFE and  $Np_1F$  (0.75 M)/BTFE:2,6-DFP (1:2) are 2.35 mS/cm and 3.85 mS/cm respectively at 25 °C (an increase of 60% in the mixture). This inspired us to investigate co-solvent mixtures with  $Np_1F$ /BTFE further (Fig. 5).

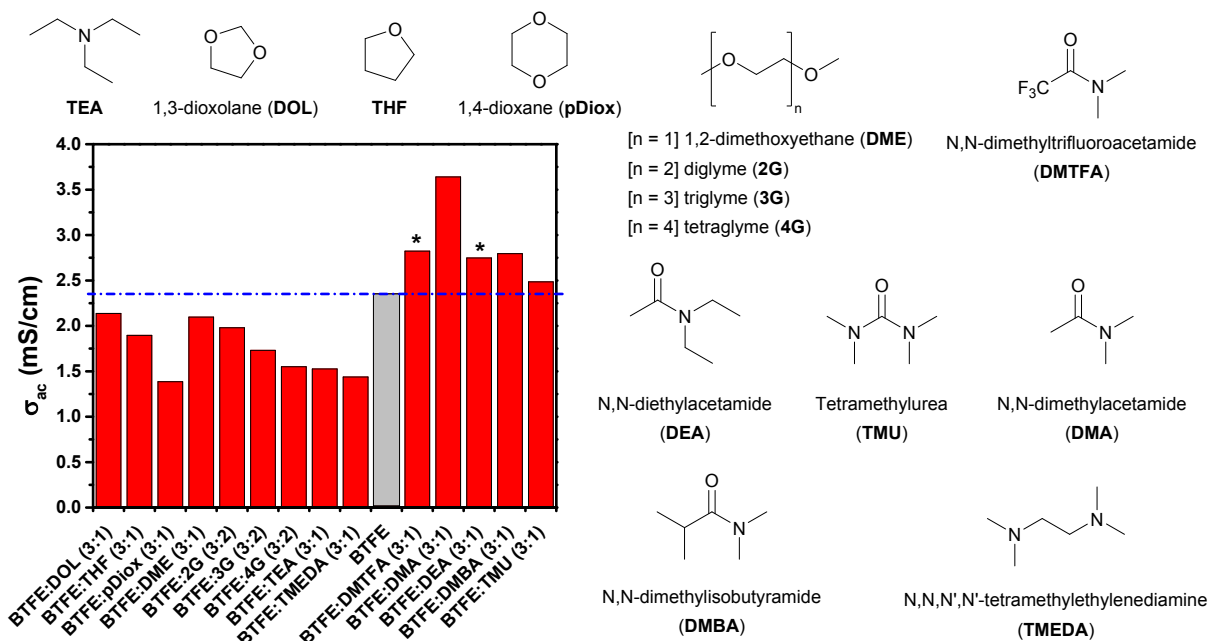


**Figure 5.** Ionic conductivity of  $Np_1F$  (0.75 M) in BTFE:co-solvent mixtures. Asterisks indicate that a color change was observed during the experiment, suggesting reaction of  $F^-$  with the co-solvent.

Of the co-solvents investigated, all the ethers and amines universally decreased ionic conductivity compared to that of 100% BTFE. In contrast, amides served to increase the measured values. In certain cases (DMTFA and DEA)  $F^-$  was found to react with the co-solvent during the experiment, although DMA, DMBA, and TMU-containing mixtures were chemically stable and exhibited improved ionic conductivity.

Computational investigation into ion–ion and ion–solvent interactions was carried out for selected 0.75 M  $Np_1F$  BTFE:co-solvent electrolyte mixtures. Analysis of the simulation results provides insight into the diffusive dynamics and  $F^-$  solvation environment of the mixtures (Table 3).

**Table 3.** Diffusion constants, ion dissociation, and  $F^-$  solvation sheath composition,  $(BTFE)_x-(co-solvent)_y-(Np_1^+)_z$ , in 0.75 M  $Np_1F$  electrolytes determined from all-atom simulations. Statistical errors for the last digit are indicated in parenthesis.

Electrolyte	$D_F$ ( $\text{\AA}^2/\text{ns}$ )	$D_{Np}$ ( $\text{\AA}^2/\text{ns}$ )	$D_{BTFE}$ ( $\text{\AA}^2/\text{ns}$ )	$D_{Co-solvent}$ ( $\text{\AA}^2/\text{ns}$ )	$\alpha^a$	$X^b$	$Y^c$	$Z^d$
BTFE (100%)	9 (1)	9 (1)	67 (3)	—	0.0022 (9)	2.64 (8)	—	2.45 (8)
BTFE:DMA (3:1)	8 (2)	7 (2)	46 (1)	53 (4)	0.082 (5)	2.17 (5)	0.50 (2)	2.53(6)
BTFE:DMBA (3:1)	6.4 (7)	6.0 (4)	53.5 (3)	53 (2)	0.02 (3)	2.4 (2)	0.18 (2)	2.3 (2)
BTFE:TEA (3:1)	6.7 (6)	6.4 (6)	73 (1)	87.0 (6)	0.002 (3)	1.93 (5)	0.026 (7)	3.13 (7)

<sup>a</sup>Degree of ion dissociation, determined from computational calculations (see ESI). <sup>b</sup>Number of BTFE molecules in the  $F^-$  solvation sheath. <sup>c</sup>Number of co-solvent molecules in the  $F^-$  solvation sheath. <sup>d</sup>Number of  $Np_1^+$  ions in the  $F^-$  solvation sheath.

As is detailed in the ESI, the experimentally observed trends in conductivity likely emerge from a competition between the effects of changing viscosity and changing ion-pairing *via* the co-solvent, and this is supported by the calculations. The changes in calculated conductivities of three of the mixtures (BTFE+DMA, DMBA, or pDIOX) were dominated by enhanced or suppressed correlation in the ion motion. In the fourth mixture (BTFE+TEA), viscosity effects dominated the change in conductivity. The relative ordering of the calculated mixture conductivities is consistent with experimental observations in all cases; however, more accurate computational prediction of the absolute conductivity values would require potential energy functions that are more accurate than the simple point-charge potentials employed here.<sup>17–19</sup>

Molecules or ions are counted as part of the solvation sheath if they provide at least two hydrogens within 3 Å of a single fluoride ion, as determined from the first peak of the radial distribution function. Results show that all co-solvent molecules barely participate in solvation of F<sup>-</sup>, as reflected by experimental observations; that is, the pure co-solvents are not able to dissolve the Np<sub>1</sub>F salt in the absence of BTFE. Similar numbers of Np<sub>1</sub><sup>+</sup> ions and BTFE molecules in the F<sup>-</sup> solvation sheath indicate that all of these mixtures exhibit substantial ion-pairing and aggregation, consistent with prior results from diffusion-ordered NMR spectroscopy.<sup>11</sup> Our simulation results further show that “good” amide co-solvents participate more in the solvation sheath than TEA (a representative “poor” co-solvent), but still remain the minority solvent molecule (Table 3). DMA and DMBA co-solvents thus improve ion dissociation by an order of magnitude compared to 100% BTFE electrolyte. These results indicate that DMA and DMBA partition between Np<sub>1</sub><sup>+</sup> cations and F<sup>-</sup> anions, creating better ionic separation, reducing ion-pairing and facilitating improved ionic conductivity.

We used the inverse of the calculated BTFE diffusion coefficient as measure of viscosity of the mixture, *via* the Stokes-Einstein equation.<sup>20</sup> For most of the mixtures investigated, the BTFE diffusion coefficient varies in a similar manner to the individual ions. The exception is for the TEA-containing mixture, which exhibits particularly high ion pairing ( $Z = 3.13$ ). As seen in Fig. S10, increases in the simulated conductivities result from reduced correlation in the ion motion, which itself stems from increased ion dissociation (Table 3). Table S4 further indicates the effect of correlation in ion motion on the mixture conductivities; neglecting correlated motion (by considering the “Nernst-Einstein” conductivity) fails to qualitatively predict the experimentally observed trends in mixture conductivity. Thus, we conclude that the experimentally-observed trends reflect a delicate balance between the factors of co-solvent-induced changes in viscosity and ion pairing.

## Conclusions

We investigated the solubility of a representative dry alkylammonium fluoride salt, Np<sub>1</sub>F, in a wide range of non-aqueous solvents with the aim of using the resulting solutions as electrolytes for FIBs. Solvent stability to F<sup>-</sup> reactivity was monitored *via* <sup>1</sup>H and <sup>19</sup>F NMR

spectroscopy. Computational studies reveal that the  $pK_a$  of solvent protons dictates  $F^-$  reactivity *via*  $HF_2^-$  formation. We found that partially fluorinated (in particular, ether-type) solvents demonstrate the highest degree of fluoride salt dissolution, most significantly when the solvent features both a favorable partial charge distribution and conformational flexibility. Three organic solvents capable of dissolving  $Np_1F$  to give stable solutions of  $F^-$  are PN, 2,6-DFP, and BTFE. While 2,6-DFP facilitates better fluoride-ion mobility than BTFE, BTFE can solubilize a greater amount of  $Np_1F$  salt. Electrolyte mixtures of BTFE with amide co-solvents exhibit improved ionic conductivity beyond the neat solvent. Simulation results indicate that such amide co-solvents facilitate better separation of the  $Np_1^+$  cations and  $F^-$  anions, and that that ion conduction trends observed for the co-solvent mixture depend upon the competing effects of viscosity and ion pairing.

## Conflicts of interest

There are no conflicts to declare.

## Acknowledgements

This work was carried out at the Jet Propulsion Laboratory, California Institute of Technology, under contract with the National Aeronautics and Space Administration. TFM, RHG and SCJ acknowledge support from the Honda Research Institute, USA; TFM also acknowledges support from the Office of Naval Research (Award N00014-10-1-0884). VKD acknowledges support from the JPL Year Round Internship Program. SM acknowledges support from a California AGEP fellowship. This research also used resources of the National Energy Research Scientific Computing Center (NERSC), a DOE Office of Science User Facility supported by the DOE Office of Science under contract DE-AC02-05CH11231.

## References

- 1 F. Gschwind, G. Rodriguez-Garcia, D. J. S. Sandbeck, A. Gross, M. Weil, M. Fichtner and N. Hörmann, *J. Fluor. Chem.*, 2016, **182**, 76–90.
- 2 I. Mohammad, R. Witter, M. Fichtner and M. A. Reddy, *ACS Appl. Energy Mater.*, 2018, **1**, 4766–4775.
- 3 I. Mohammad, R. Witter, M. Fichtner and M. A. Reddy, *ACS Appl. Energy Mater.*, 2019, **2**, 1553–1562.
- 4 K. O. Christe, W. W. Wilson, R. D. Wilson, R. Bau and J. A. Feng, *J. Am. Chem. Soc.*, 1990, **112**, 7619–7625.
- 5 H. Sun and S. G. Dimagno, *J. Am. Chem. Soc.*, 2005, **127**, 2050–2051.
- 6 S. J. Ryan, S. D. Schimler, D. C. Bland and M. S. Sanford, *Org. Lett.*, 2015, **17**, 1866–1869.
- 7 S. Elias, N. Karton-Lifshin, L. Yehezkel, N. Ashkenazi, I. Columbus and Y. Zafrani, *Org. Lett.*, 2017, **19**, 3039–3042.
- 8 F. Gschwind, Z. Zao-Karger and M. Fichtner, *J. Mater. Chem. A*, 2014, **2**, 1214–1218.
- 9 H. Konishi, T. Minato, T. Abe and Z. Ogumi, *J. Electrochem. Soc.*, 2017, **164**, A3702–A3708.
- 10 W. Liu, A. G. Oliver and B. D. Smith, *J. Org. Chem.*, 2019, **84**, 4050–4057.
- 11 V. K. Davis, C. M. Bates, K. Omichi, B. M. Savoie, N. Momčilović, Q. Xu, W. J. Wolf, M. A. Webb, K. J. Billings, N. H. Chou, S. Alayoglu, R. K. McKenny, I. M. Darolles, N. G. Nair, A.

- Hightower, D. Rosenberg, M. Ahmed, C. J. Brooks, T. F. Miller, R. H. Grubbs and S. C. Jones, *Science (80-. )*, 2018, **362**, 1144–1148.
- 12 F. Neese, *Wiley Interdiscip. Rev. Comput. Mol. Sci.*, 2012, **2**, 73–78.
- 13 F. R. Manby, T. F. Miller III, P. J. Bygrave, F. Ding, T. Dresselhaus, F. A. Batista-Romero, A. Buccheri, C. Bungey, S. J. R. Lee, R. Meli, K. Miyamoto, C. Steinmann, T. Tsuchiya, M. Welborn, T. Wiles and Z. Williams, *ChemRxiv.7762646*.
- 14 K. Xu, *Chem. Rev.*, 2014, **114**, 11503–11618.
- 15 K. O. Christe and W. W. Wilson, *J. Fluor. Chem.*, 1990, **47**, 117–120.
- 16 F. G. Bordwell, J. E. Bares, J. E. Bartmess, G. E. Drucker, J. Gerhold, G. J. McCollum, M. Van Der Puy, N. R. Vanier and W. S. Matthews, *J. Org. Chem.*, 1977, **42**, 326–332.
- 17 A. France-lanord and J. C. Grossman, *Phys. Rev. Lett.*, 2019, **122**, 1–6.
- 18 C. J. Fennell, A. Bizjak, V. Vlachy and K. A. Dill, *J. Phys. Chem. B*, 2009, **113**, 6782–6791.
- 19 B. M. Savoie, M. A. Webb and T. F. Miller, *J. Phys. Chem. Lett.*, 2017, **8**, 641–646.
- 20 J. P. Hansen and I. R. McDonald, *Theory of Simple Liquids*, Academic Press, Inc., London, 2nd edn., 1990.

Copyright 2019. All rights reserved.